Diode Characterization of Rockwell LWIR HgCdTe Detector Arrays

Candice M. Bacon[a], Judith L. Pipher[a], William J. Forrest[a], Craig W. McMurtry[a] and James D. Garnett[b]

[a]University of Rochester, Rochester, NY, USA
[b]Rockwell Scientific Company, Camarillo, CA, USA

ABSTRACT

Future infrared space missions will undoubtedly employ passively cooled focal planes (T $\sim$ 30K), as well as passively cooled telescopes. Most long-wave detector arrays (e.g. Si:As IBC) require cooling to temperatures of $\sim 6-8$K.[1] We have been working with Rockwell to produce 10μm cutoff HgCdTe detector arrays that, at temperatures of $\sim$ 30K, exhibit sufficiently low dark current and sufficiently high detective quantum efficiency to be interesting for astronomy. In pursuit of these goals, Rockwell Scientific Company has delivered twelve 256×256 arrays (several of them engineering arrays), with cutoff wavelengths at 30K between 7.4 and 11μm for characterization at Rochester. Seven of these arrays utilize advanced structure diodes with differing capacitances arranged in rows (banded arrays), and the materials properties of the HgCdTe also vary significantly from array to array. Of ultimate interest to astronomy is the fraction of pixels with dark current below the target value of $\sim 100e^-/s$ with 10-60mV of actual reverse bias across the diodes at T $\sim$ 30K. These arrays were developed for the purpose of selecting diode architecture: we use this fraction as one criterion for selection. We have determined from these experiments the optimal diode architecture for future array development. Measurement of the dark current as a function of reverse bias and temperature allows us to ascertain the extent to which trap-to-band tunneling dominates the dark current at this temperature. We present the results for one representative array, UR008.

Keywords: Long Wave InfraRed (LWIR) Detector, HgCdTe, Dark Current, Diode Characterization, Infrared Space Missions

1. INTRODUCTION

In an effort to enable low-cost, long-lived, future infrared space missions, long wavelength detector arrays must be able to function without active cooling. Rather than employing cryogens or mechanical coolers, future telescopes in space, with proper design, will employ passive cooling, and will be able to attain focal plane temperatures of 25 to 30K. Therefore, we have been pursuing development of long wavelength HgCdTe detector arrays that will exhibit low dark current and relatively high quantum efficiencies in this temperature range.

Rockwell Scientific Company has developed a molecular beam epitaxy (MBE) Double Layer Planar Heterostructure (DLPH) process[2] which eliminates, to a large extent, surface dark currents. We have reported[3,4] that 10.6μm HgCdTe single pixel devices, with doping $\sim 9.5 \times 10^{14} cm^{-3}$, showed excellent performance at 30K where 8 of the 17 single diodes tested exhibited low dark currents (dominated by trap to band tunneling) for their size and applied bias. The Rockwell advanced structure junctions (junction area < optical area, so that G-R currents and capacitance are minimized) were the best performing diodes in the lot.

Our ultimate goal is to have Rockwell produce 10μm cut-off detector arrays with sufficiently low dark current that they are astronomically interesting, while exhibiting excellent pixel operability and uniformity, as well as adequate well depth and quantum efficiency. In an effort to reach these goals, Rockwell has delivered, in the past year and a half, a series of seven banded 256×256 LWIR HgCdTe detector arrays, bonded to engineering grade NICMOS3 multiplexers. These were best effort deliveries with no guarantee that our low dark current

Further author information:
E-mail: candice@astro.pas.rochester.edu

goal would be achieved for a high percentage of the pixels. Each device includes a number of different diode geometries in order to ascertain the optimal diode choice for future arrays. In addition, the characteristics of the base material (doping, cut-off wavelength, microdefects, voids, etch pitch density, mobility) for each deliverable varied. We report here on one of those arrays, UR008, a 9.3μm wavelength cut-off device (at 30K), with relatively high doping ($1.6 \times 10^{15} cm^{-3}$) and hence lower G-R current, all other parameters remaining the same.

2. GOALS

The dark current requirements for a space astronomy experiment are driven by background radiation levels in space. At $\lambda < 30\mu$m, the dominant background emission in space is from the zodiacal dust cloud. The zodiacal background radiation was measured by the COBE (Cosmic Background Explorer) experiment. At the south ecliptic pole, where this background is at a minimum, COBE measured $\lambda I_\lambda = 7$ to $30 \times 10^{-11} W/cm^2 sr$ at wavelengths 5.5 to 10μm. The resulting photo-current per diffraction-limited pixel at spectral resolution $R = 3$ ($R = \lambda/\Delta\lambda$), is given in Figure 1. From this figure, we see that for 10μm or 5μm background-limited space operation, at $R = 3$, we require dark currents $< 2000 e^-/s$/pixel or $30 e^-/s$/pixel respectively. Since InSb covers the wavelength range out to 5.3μm at focal plane temperatures of 30K well, we concentrate here on dark currents $< 100 e^-/s$/pixel.

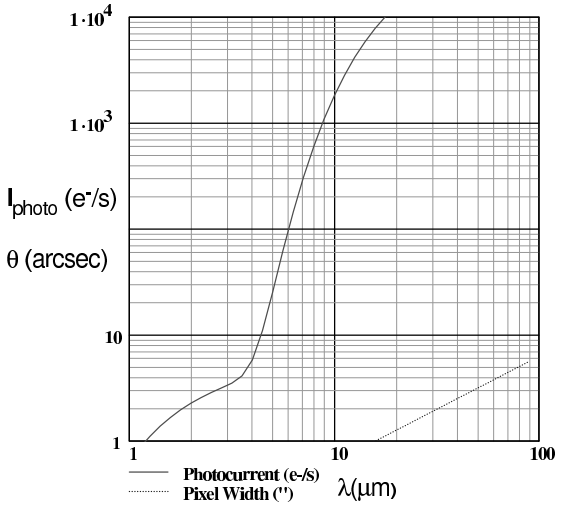

Figure 1. Zodiacal Light emission levels for diffraction limited pixels, QE = 70%, optical efficiency 48%, and spectral resolution $R = 3$. The diffraction-limited pixel width (here $1.22\lambda/D$) is shown for a D = 4m telescope.

In past experiments we have shown that relatively low doping in conjunction with Double Layer Planar Heterostructure (DLPH) HgCdTe technology utilized at the Rockwell Scientific Company should reduce tunneling dark currents to below the target dark current in the best diodes.[3] In the best case, we would hope to be limited by G-R currents, which for $< 100 e^-/s$ requires temperatures $\leq$ 30K. The dark current results for UR008 will be discussed in Section 4.1.

High pixel operability and uniformity are also necessary: an operable pixel will meet the dark current specification, and in addition exhibit adequate quantum efficiency (for comparison, Raytheon Si:As IBC arrays exhibit a detective quantum efficiency of $\sim 50\%$[1]). However, these operability/uniformity goals were not the direct objective of this program: nonetheless, we have, in this 9.3μm cut-off wavelength array, achieved our dark current goal for a sizeable fraction of pixels for specific diode geometries. The well depth must also be adequate for the scientific application, and the cut-off wavelength can be tailored to that application. Of course, the longer the cut-off wavelength, the higher the limiting G-R currents for a given array temperature.

3. DIODE PRELIMINARIES

Each of the seven banded deliveries from Rockwell are configured such that testing of multiple diode structures can be done on one array. Each array has nine different sizes/geometries of diode implants arranged in rows, which will be identified as type A through I throughout the rest of this paper. The array begins with type A for four rows and then type B for four rows and so on until type I, after which the pattern starts over again with type A. This leads to 8192* pixels of type A and 7168 pixels of all subsequent types. The image in Figure 2 shows the arrangement by rows of diode types A through I in successively lighter shades of grey.

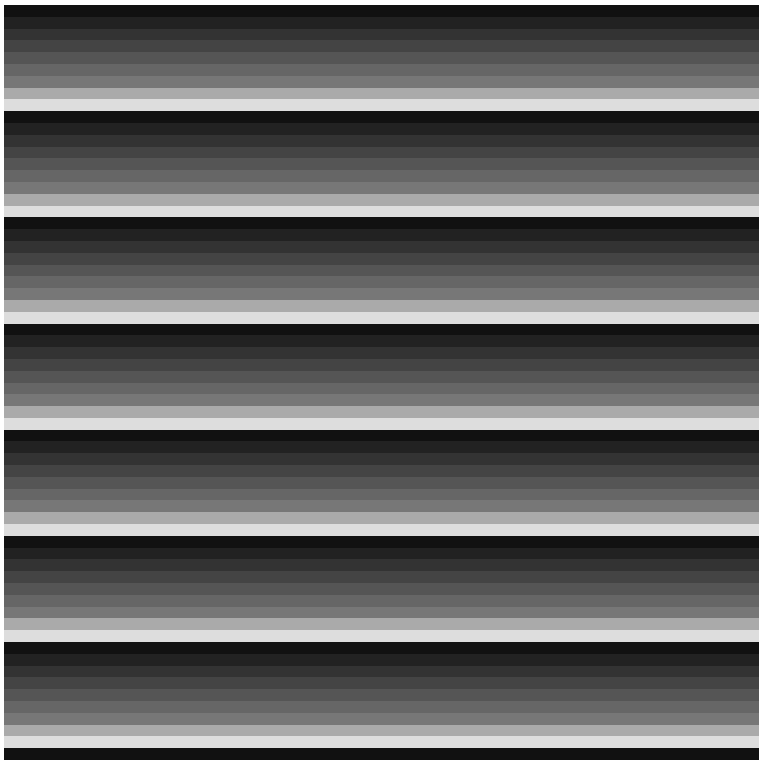

Figure 2. This image shows the pattern of the sequential rows of diodes of varying geometries.

For types A through G the capacitances were estimated. Types H and I were not included here because their diode configurations proved inappropriate to our program. The capacitances as well as the e^-/ADU for our system are given in Table 1.

4. TESTING AND RESULTS

4.1. Dark Current Measurements

The dark current goal for this set of detectors was $< 100e^-/s$ at a focal plane temperature of T $\sim$ 30K. We employed correlated triple sampling mode to obtain these measurements with external light blocked by a liquid helium cooled, blackened aperture stop. The measurements were taken at an actual reverse bias of 60mV (corresponding to 0mV applied bias). Figure 3 is a graph showing the *mean* dark charge vs. integration time for each pixel type. An appropriate one second bias frame value has been subtracted from each datum. Each mean includes pixels that met our goal of $< 100e^-/s$ in a bias frame subtracted 100 second integration frame.

*Row 1 and row 256 (both type A) were omitted in data reduction because their performance was not consistent with the rest of the array. This leads to 7680 total available pixels in Table 3.

Table 1. Estimated capacitances of the various types followed by the number of electrons per ADU (Analog to Digital Unit) for our system.

Type	Capacitance (fF)	e^-/ADU
A	84	16.7
B	87	17.2
C	90	17.8
D	95	18.8
E	100	20.2
F	110	22.3
G	130	25.5

We excluded from the means hot pixels and pixels with very high dark current, which might exhibit close to zero mean difference. Those pixels meeting the goal and satisfying the above constraints are white in the pixel mask shown in Figure 4.

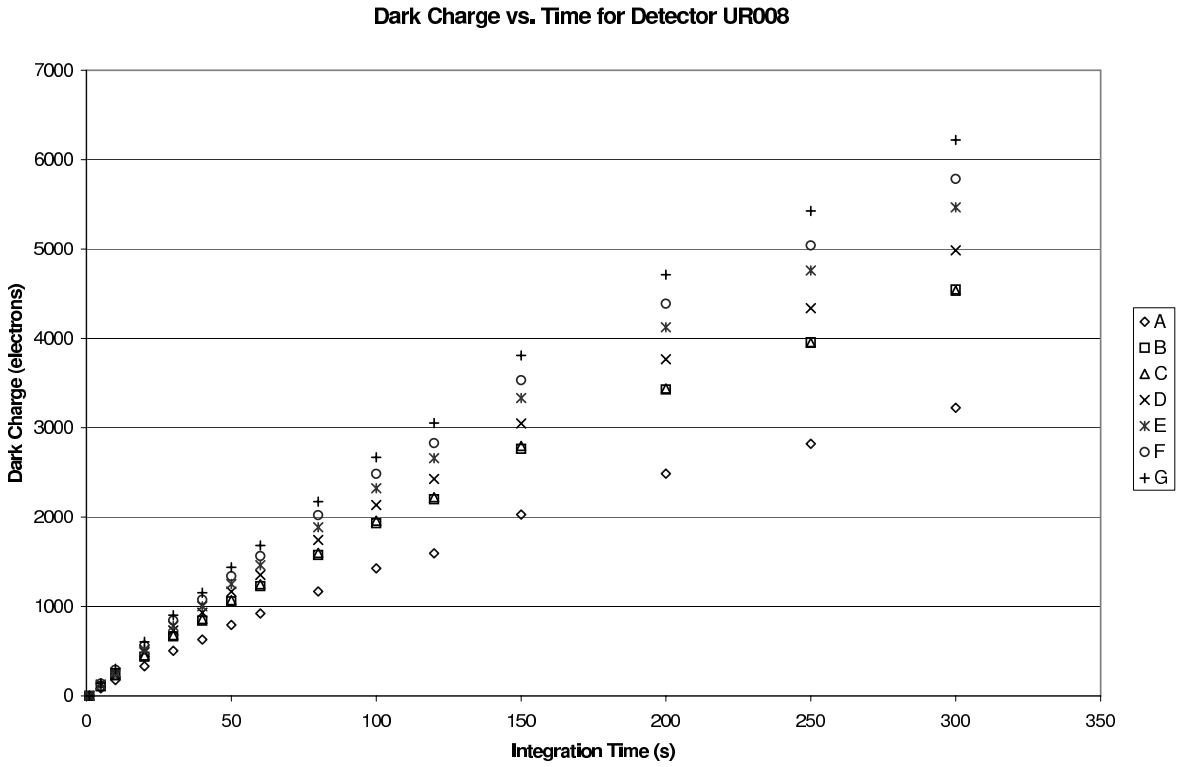

Figure 3. This graph shows the dark charge vs. time for deliverable UR008 at a temperature of 32.6K with 60mV of reverse diode bias.

A linear fit to the data in Figure 3 from 100 seconds to 300 seconds integration time gives the slope (dark current), reported in Table 2. The dark charge data are nonlinear at short integration times. Note that the mean dark current for the good pixels for all of these pixel types is much less than the goal. The dark current has also been measured at two other applied biases, 50mV and 100mV (110mV and 160mV actual reverse bias). In diode types A, B, and C, the best three geometries, the dark current doubled with each 50mV increment in applied bias. This suggests only a modest tunneling component to the dark current.[3] In fact, our estimates of

Table 2. Mean dark current for each diode type.

Type	Dark Current (e^-/s)
A	9
B	13
C	13
D	14
E	16
F	16
G	18

the G-R current for reasonable assumptions on the minority carrier lifetime are of the same order of magnitude as the measured dark currents.

4.2. Fraction of Pixels meeting Low Dark Current Goals

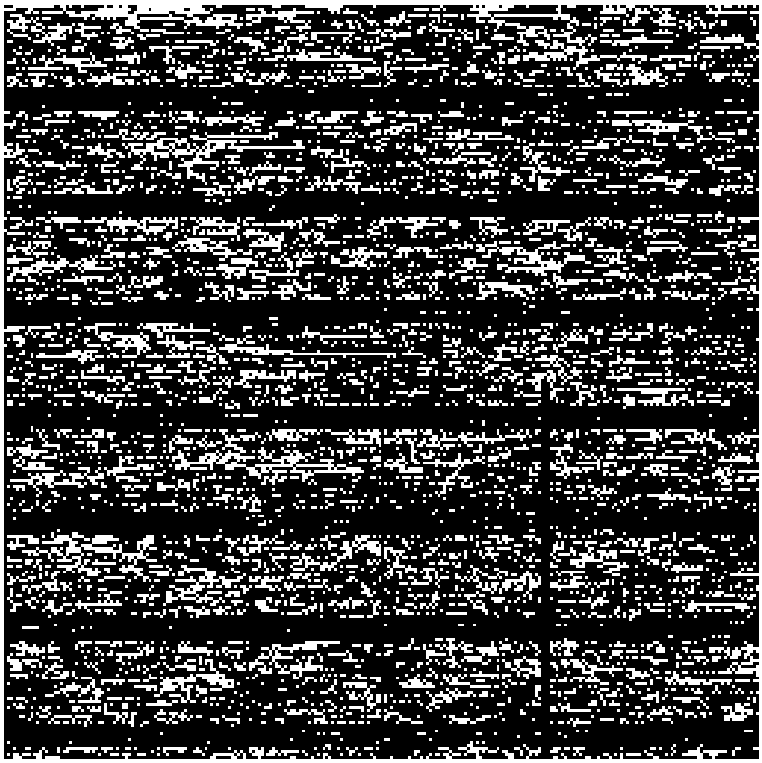

Figure 4. This image shows the pixels with dark current below the stringent goal of $100e^-/s$ in white and above that goal in black. We emphasize that this goal was **not** a requirement. Artifacts of the engineering muxes are also apparent: e.g. see the vertical black bar.

The fraction of low dark current pixels in Rockwell deliverable UR008, a 9.3μm cut-off array, is shown in Figure 4. As seen in the figure, the very small fraction of types H and I meeting these low dark current goals are indicated by the black bands. Table 3 shows the percentage of low dark current pixels for each diode geometry. From Tables 2 and 3, we find diode type A gives the best dark current performance.

Table 3. Percentage of Low Dark Current Pixels vs. Diode Type

Type	Number of Pixels	Total Available	Percentage
A	2590	7680	34
B	1998	7168	28
C	2195	7168	31
D	2138	7168	30
E	1953	7168	27
F	1799	7168	25
G	1830	7168	25
H	161	7168	2.2
I	168	7168	2.3

4.3. Well Depth

The available well depth for each diode type was determined based upon the capacitance of the particular geometric configuration of the diode. The image mask shown in Figure 4 was used to select those pixels for which we obtain the well depth. For this experiment, a small photo-signal was used to integrate to saturation. (The photo-signal is small to minimize the degree of forward bias at saturation). The graph in Figure 5 shows the photo-signal vs. time as the detector array UR008 integrates to saturation at an applied bias of 0mV. The

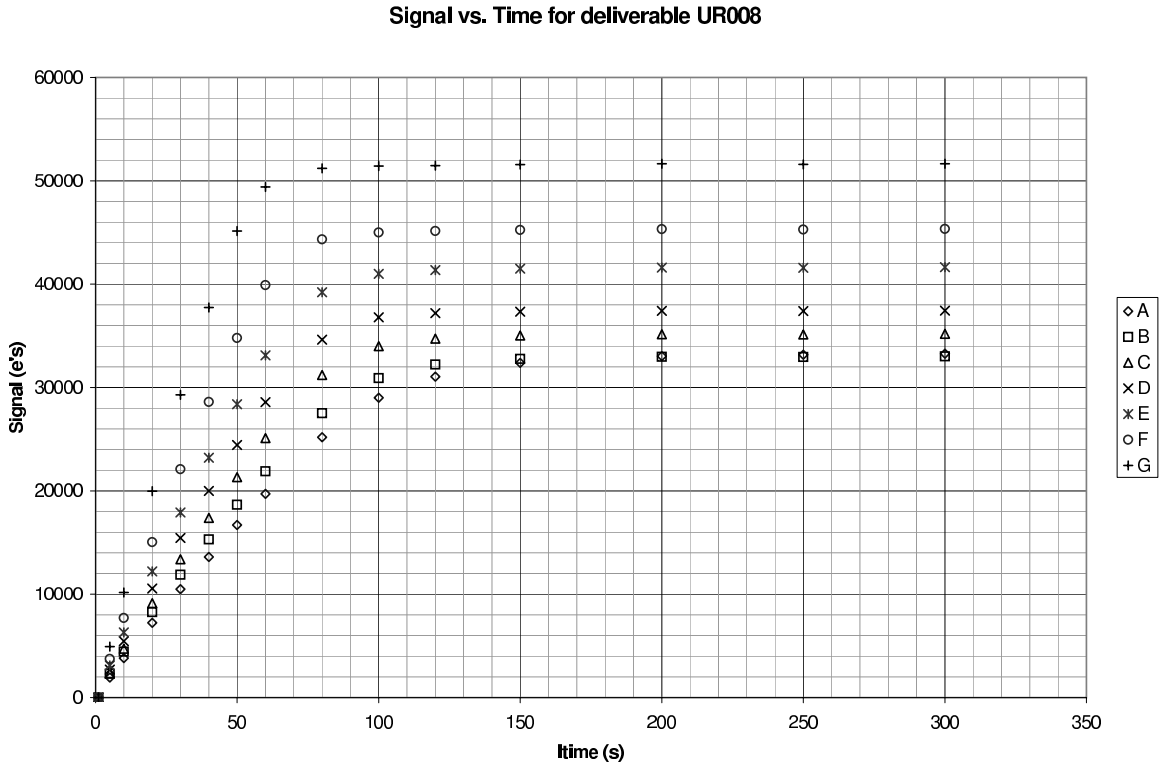

Figure 5. This graph shows the signal vs. time for deliverable UR008 at a temperature of 31.7K. Signal is combined photo-charge and dark charge. Applied bias = 0mV, corresponding to 60mV reverse bias at the beginning of the integration ramp.

saturation level, i.e. the amount of actual reverse bias ($\sim$ 60mV) across the diodes at the beginning of the integration ramp, is tabulated below in Table 4.

Table 4. Saturation Level vs. Pixel Type

	Saturation Level		
Type	ADU	e^-	mV
A	1960	34500	59.8
B	1910	34600	58.3
C	1950	36700	59.6
D	1960	39000	59.9
E	2030	43300	62.1
F	2010	47200	61.2
G	1990	53700	60.8
H	1970		60.2
I	1900		58.0

4.4. Relative Quantum Efficiency

The relative quantum efficiency as a function of wavelength was obtained by measuring the response of those detector pixels selected as low dark current pixels, as a function of wavelength from 8μm to approximately

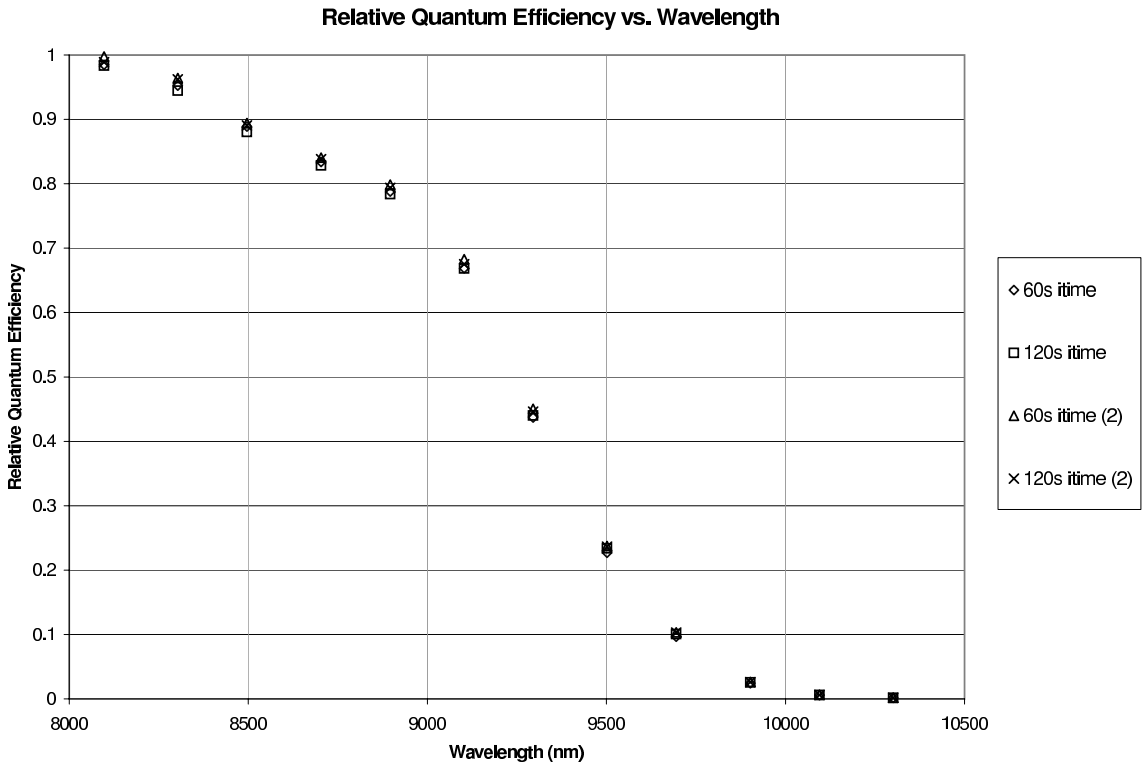

Figure 6. This graph shows the relative quantum efficiency for deliverable UR008 at a temperature of 33K for 0mV applied bias (60mV reverse bias) across the array.

12μm, defined by a cold circular variable filter of $\sim$ 1.54% resolution. These data were taken as follows. The array UR008 viewed a blackened metal plate on the liquid nitrogen shield of the dewar through a liquid helium cooled Lyot stop of 2mm diameter, and the signal, which consisted of photo-charge and dark charge, was then dark-subtracted to yield the photo-signal. This was compared against the expected grey-body signal from the liquid nitrogen cooled black plate, which is at T $\sim$ 80K, assuming a value for the emissivity at these wavelengths, and 100% fill factor. Because there is uncertainty in the temperature of the black plate, the emissivity (assumed grey), and the optical area of the pixels, only the relative quantum efficiency has been measured and is shown normalized to unity in Figure 6.

4.5. Cutoff Wavelength

The cutoff wavelength for this device is defined as the half-power point of the detector response. This point is reached at about 9.3μm for a focal plane temperature of 30K, based upon the relative quantum efficiency (see Figure 6).

5. CONCLUSIONS

Although there are many variable parameters in the determination of good HgCdTe material for low dark current LWIR detectors, it is clear that remarkably low dark current HgCdTe LWIR arrays, suitable for ultralow backgrounds in space astronomy, are becoming possible. Choices among diode geometries have been made from these experiments. Diode type A (and perhaps types B and C), due to their superior dark current performance for a substantial fraction of the pixels, will be the primary focus of future deliveries. We will work with Rockwell to improve further the fraction of good pixels in future deliveries.

UR008 appears to exhibit close to G-R limited performance in a substantial fraction of pixels in the array. This result represents a breakthrough in materials processing over ultralow background application LWIR HgCdTe we have tested at Rochester in the past.

ACKNOWLEDGMENTS

We are grateful for support for this program. Specifically we acknowledge NASA grants NAG5-6267 and NAG5-8642, as well as NASA Ames grant NAG2-1280.

REFERENCES

1. A. D. Estrada, G. Domingo, J. D. Garnett, A. W. Hoffman, N. A. Lum, P. J. Love, S. L. Solomon, J. E. Venzon, G. R. Chapman, K. P. Sparkman, C. R. McCreight, M. E. McKelvey, R. E. McMurray, J. A. Estrada, S. Zins, R. McHugh, and R. Johnson, "Si:As IBC IR focal plane arrays for ground-based and space-based astronomy," in *Proc. SPIE Vol. 3354, p. 99-108, Infrared Astronomical Instrumentation, Albert M. Fowler; Ed.*, **3354**, pp. 99–108, Aug. 1998.
2. J. M. Arias, J. G. Pasko, M. Zandian, S. H. Shin, G. M. Williams, L. O. Bubulac, R. E. Dewames, and W. E. Tennant, "Planar p-on-n HgCdTe heterostructure photovoltaic detectors," *Applied Physics Letters* **62**, pp. 976–978, Mar. 1993.
3. J. Wu, *Development of Infrared Detectors for Space Astronomy, PhD Thesis*, University of Rochester, Rochester, NY, 1997.
4. R. B. Bailey, J. M. Arias, W. V. McLevige, J. G. Pasko, A. C. Chen, C. Cabelli, L. J. Kozlowski, K. Vural, J. Wu, W. J. Forrest, and J. L. Pipher, "Prospects for large-format IR astronomy FPAs using MBE-grown HgCdTe detectors with cutoff wavelength $> 4\mu$m," in *Proc. SPIE Vol. 3354, p. 77-86, Infrared Astronomical Instrumentation, Albert M. Fowler; Ed.*, **3354**, pp. 77–86, Aug. 1998.